from the BIR-1 standard. All Fe isotope data listed in Table 1 are precise to 0.2 per mil or less at the 95% confidence level and represent the average of two complete procedural runs per sample.

30. The ratio of isotopic rate constants for ^{54}Fe and ^{56}Fe (k_{54}/k_{56}), referred to as the kinetic fractionation factor (kff), was calculated for the three experiments listed in Table 1 that have both Fe isotope and solution concentration data. This calculation assumes a Rayleigh distillation process controlled by a simple one-step first-order reaction. The kff was calculated according to the following equation, provided by Krouse and Tabatabai [H. R. Krouse and M. A. Tabatabai, in *Sulfur in Agriculture*, vol. 27 of *Agronomy Monograph Series*, M. A. Tabatabai, Ed. (American Society of Agronomy, Madison, WI, 1986), pp. 169–205]: $k_{54}/k_{56} = \ln(1 - F)/\ln(1 - rF)$, where F is the fraction of substrate reacted $\{1 - ([Fe]_{final}/[Fe]_{initial})\}$ and r is $(^{56}Fe/^{54}Fe_{AccumulatedProduct})/(^{56}Fe/^{54}Fe_{InitialReactant})$. Calculated values of kff are 0.99979 for strain MV-1 with chelator and 0.99971 for strain MV-1 without chelator, which correspond, respectively, to a 0.21 and 0.29 per mil instantaneous relative enrichment of ^{56}Fe in the Fe_3O_4 product. The calculated value is 1.00026 for strain MS-1 with chelator, which corresponds to a 0.26 per mil instantaneous relative depletion of ^{56}Fe in the Fe_3O_4 product. These values are only slightly greater than the maximum 2σ precision of 0.2 per mil for the Fe isotope compositions reported in Table 1, and we suggest that this level of apparent fractionation is insignificant and not convincingly resolvable with our current analytical technique. Furthermore, the Fe isotope compositions of all product-reactant pairs listed in Table 1 are essentially identical within 95% confidence limits.

31. D. Schueler and E. Baeuerlein, *Arch. Microbiol.* **166**, 301 (1996).
32. R. H. Becker and R. N. Clayton, *Geochim. Cosmochim. Acta* **40**, 1153 (1976).
33. M. W. Rowe, R. N. Clayton, T. K. Mayeda, *ibid.* **58**, 5341 (1994).
34. Y. Zheng, *ibid.* **55**, 2299 (1991).
35. J. R. O'Neil and R. N. Clayton, in *Isotopic and Cosmic Chemistry*, H. Craig, S. L. Miller, G. J. Wasserburg, Eds. (North Holland, Amsterdam, 1964), pp. 157–168.
36. P. Blattner, W. R. Braithwaite, R. B. Glover, *Isot. Geosci.* **1**, 195 (1983).
37. S. Mann, N. H. C. Sparks, V. J. Wade, in *Iron Biominerals*, R. B. Frankel and R. P. Blakemore, Eds. (Plenum, New York, 1990), pp. 21–49.
38. K. A. Short and R. P. Blakemore, *J. Bacteriol.* **167**, 729 (1986).
39. L. C. Paoletti and R. P. Blakemore, *Curr. Microbiol.* **17**, 339 (1988).
40. W. F. Guerin and R. P. Blakemore, *Appl. Environ. Microbiol.* **58**, 1102 (1992).
41. Y. Zheng, *Chem. Geol.* **121**, 309 (1995).
42. G. Wefer and W. H. Berger, *Mar. Geol.* **100**, 207 (1991).
43. D. A. Bazylinski, A. J. Garratt-Reed, R. B. Frankel, *Microsc. Res. Tech.* **27**, 389 (1994).
44. C. J. Yapp, *Chem. Geol.* **85**, 329 (1990).

45. We thank R. Frankel, M. Fogel, C. Johnson, B. Rye, M. Wahlen, Y. Gorby, and B. Hoyle for helpful discussions about this project and P. Gemery and T. Pulsipher for technical support. D.A.B. is supported by NSF grant CHE-9714101 and NASA Johnson Space Center grant NAG 9-1115.

8 April 1999; accepted 22 July 1999

Optical Measurements of Invasive Forces Exerted by Appressoria of a Plant Pathogenic Fungus

Clemens Bechinger,[1] Karl-Friedrich Giebel,[1] Martin Schnell,[1] Paul Leiderer,[1] Holger B. Deising,[3]* Martin Bastmeyer[2]*

Many plant pathogenic fungi, such as the cereal pathogen *Colletotrichum graminicola*, differentiate highly specialized infection structures called appressoria, which send a penetration peg into the underlying plant cell. Appressoria have been shown to generate enormous turgor pressure, but direct evidence for mechanical infection of plants by fungi is lacking. A microscopic method was developed that uses elastic optical waveguides to visualize and measure forces locally exerted by single appressoria. By this method, the force exerted by appressoria of *C. graminicola* was found to be about 17 micronewtons.

Plant pathogens are estimated to cause a reduction in yield of almost 20% in worldwide food and cash crops (*1*). Among these pathogens are fungi that invade plant cells to gain access to nutrients. Some fungal pathogens, such as members of the genera *Colletotrichum* or *Magnaporthe*, differentiate highly specialized infection structures called appressoria with rigid melanin-pigmented cell walls. Appressoria adhere tightly to the leaf surface of the host and develop an enormous turgor pressure by synthesizing elevated intracellular concentrations of osmotically active substances. In the causal agent of rice blast, *M. grisea*, Talbot and co-workers demonstrated that the osmoticum is glycerol, which accumulates to concentrations of more than 3 M (*2*). The plant cell is then invaded by a specialized penetration hypha that develops beneath the appressorium (*3, 4*). Previous experiments have indicated that melanization and high turgor pressure are essential for pathogenicity in *Colletotrichum* and *Magnaporthe* (*3–5*). The role of extracellular enzymes in facilitating perforation of the plant cell wall is still under debate (*4, 6*). Direct measurement of the force exerted during initial penetration, rather than indirect measurement of turgor pressure, may not only help to resolve critical aspects of host pathogen interactions, but could also facilitate the development of new antipenetrant fungicides. We introduce a technique, involving light propagation in planar waveguides, that allows optical imaging and thus direct determination of vertical forces exerted by single appressoria.

Sensing techniques based on guided optical waves have been well known for many years. The Otto and Kretschmann-Raether surface plasmon configurations are well documented as reliable methods for examining dielectric constants of thin films (*7, 8*). It is the sensitivity of such electromagnetic waves to minute modifications in the sample environment that makes optical waves useful for sensor applications. The essence of the technique is the principle of total internal reflection, which occurs when light is reflected from a surface above the critical angle Θ_c. For an interface between two different layers, $\sin \Theta_c = n_2/n_1$, where n_1 and n_2 are the optical constants of the two layers. This phenomenon is also crucial for light propagation in planar waveguides composed of a layer with high refractive index (core) sandwiched between material with lower refractive index (cladding). As a result of the interfaces, which laterally confine the electromagnetic field, only well-defined modes similar to those in a Fabry-Perot interferometer can propagate within a waveguide. The modes are characterized by a resonance condition,

$$\cos \Theta_R = m\pi/dk \qquad (m = 1, 2, 3, \ldots) \tag{1}$$

where d is the waveguide thickness, k is the wave vector inside the core, Θ_R is the angle of incidence at the cladding material, and m is the mode index.

Accordingly, if laterally resolved measurements of Θ_R are performed, Eq. 1 can be used to study the topography of a waveguide with a precision in the nanometer range. If the surface of the waveguide is deformed, for example, by the influence of vertical external forces, one obtains an image of the corresponding indentation. When the elastic constants of the waveguide are known, the local force inducing the deformation can be calculated.

To determine the local thickness of optical

[1]Faculty of Physics, [2]Faculty of Biology, University of Konstanz, Fach M626, D-78457 Konstanz, Germany. [3]Faculty of Agriculture, Phytopathology and Plant Protection, Martin-Luther-University Halle-Wittenberg, Ludwig-Wucherer-Straβe 2, D-06099 Halle (Saale), Germany.

*To whom correspondence should be addressed. E-mail: martin.bastmeyer@uni-konstanz.de, deising@landw.uni-halle.de

waveguides, we used the prism-coupling technique (*9, 10*), long known as a reliable method for the characterization of multilayer structures. The planar waveguide was optically matched to the base of a prism illuminated from below with a parallel laser beam. At well-defined angles of incidence, where the evanescent field leaking into the waveguide matches its propagation constant, this mode is resonantly excited at the expense of the reflected light intensity $R(\Theta)$, which then shows a sharp dip as a function of Θ (*11*). Regions of the sample having the correct optical thickness to support an optical waveguide mode at a chosen angle of incidence will appear dark in reflection, while other areas will appear bright (Fig. 1, A and B) (*12, 13*). We sought to apply this experimental system to single living cells.

The corn pathogen *C. graminicola* was allowed to differentiate appressoria on optical waveguides. Because fungal development had to be monitored during the experiments, we constructed a miniaturized apparatus for the excitation of waveguides (Fig. 1C). The experimental setup consists of two arms holding the optical components for illuminating and imaging the base of the glass prism, which carries the waveguide. The angle between the two arms can be adjusted to obtain the condition where the guided wave resonance is observed. The beam diameter of a laser diode (3 mW, λ = 670 nm) is increased to ~5 mm by a beam expander, strikes a mirror, and is guided to the prism through a polarizer (P) by two positive lenses (Fig. 1C, lenses L1 and L2). The mirror is mounted on a motorized rotation stage controlled by a computer. This allows illumination of the same location of the prism base at defined angles of incidence when the mirror is rotated. The reflected light is projected with a microscope objective (lens L3; Zeiss Achromat LDN, 20×/0.35) and an eyepiece (lens L4; 12.5×) onto a charge-coupled device (CCD) camera chip and stored on a computer. The setup is attached to the stage of an upright microscope (Axioplan, Zeiss) equipped with epi-illuminated optics and a long-distance water-immersion lens (lens L5; Zeiss Achroplan 20×/0.5w). The image of the surface of the waveguide is focused onto a second CCD camera, which is connected to an image processing system.

The optical waveguides consist of a high-viscosity polydimethylsiloxane (PDMS) layer (*14*) sandwiched between two thin films of aluminum (Al). Of several metals tried, we found Al to provide the best chemical stability at the high-humidity conditions to which the waveguide was exposed. We first deposited a 13-nm-thick Al layer by thermal evaporation onto a glass slide to allow efficient coupling of the incident laser beam into the waveguide. Then the PDMS film was spin-cast onto the metalized substrate, resulting in uniform, highly transparent films typically 1 μm thick. After

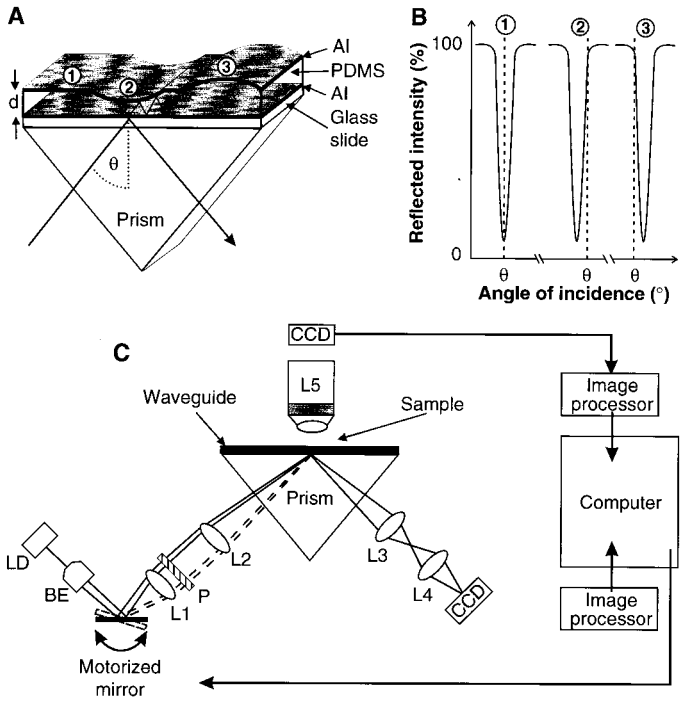

Fig. 1. (**A** and **B**) The flexible waveguide consists of a silicone layer (PDMS) sandwiched between two Al layers (A). The waveguide is prepared on a glass slide optically matched to a glass prism, which is necessary to couple light into the waveguide; *d* is the thickness of the waveguide. When the angle of incidence Θ meets the resonance condition of the waveguide, a propagating waveguide mode is excited, leading to a strong dip in the intensity of the reflected light (B). The angle of resonance strongly depends on the local thickness of the waveguide. Therefore, if the reflected light is imaged onto a camera chip at a fixed Θ (dashed lines), only those parts of the waveguide with the proper thickness (1) appear black; parts that are thinner (2) or thicker (3) appear bright. (**C**) Schematic of the experimental setup to visualize and measure locally applied forces. LD, laser diode; BE, beam expander.

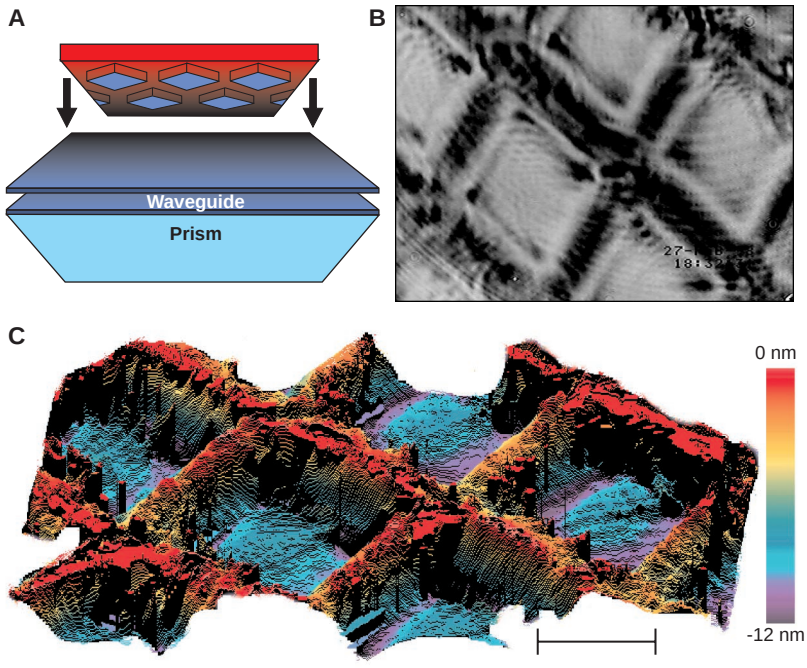

Fig. 2. (**A**) A microfabricated silicon test structure (periodically arranged protruding squares 20 μm on a side and 5 μm apart) is used to deform a planar waveguide of PDMS optically matched to a glass prism. (**B**) When the test structure is lightly pressed against the waveguide, the protruding parts deform it locally. For a fixed angle of incidence, this leads to a high-contrast video image of the reflected light. The slight deviation from the geometrical shape of the test structure is due to the tilted position of the waveguide with respect to the optical axis. (**C**) Three-dimensional reconstruction of the waveguide surface obtained from 200 video images taken at different angles of incidence. The colors correspond to the local deformation of the waveguide. These measurements show that the vertical accuracy of the method is in the nanometer range, whereas the lateral resolution is in the range of 1 to 2 μm. Scale bar, 20 μm.

spin-casting, the films were exposed to a 150-W xenon ultraviolet lamp for 2 hours. This formed a weakly cross-linked PDMS layer, which was stable enough to support a second evaporated Al layer 50 nm thick. This second metal layer was necessary to ensure optical insulation of the waveguide from the environment. The procedure resulted in a waveguide with low mechanical resistance, permitting local deformation by minute vertical forces.

The optical response of an elastic waveguide upon imprinting with a micromanufactured silicon test structure with periodically arranged square protrusions is shown in Fig. 2. Before the test pattern was pressed onto the flexible waveguide, the angle of incidence was adjusted to $\Theta = \Theta_R$, leading to a uniform, low-intensity reflected light image. At points where the stamp is in direct contact with the waveguide, the reduced thickness leads to a change in the reflected intensity, R. In contrast, in regions where no direct contact is made, no change in R was observed. The deformation of the waveguide is reversible; the reflected light image becomes uniform again immediately after the stamp is removed (*15*). We recorded images of the same location for different angles of incidence by the computer-controlled operation of the mirror (Fig. 1). In a period of 60 s, we adjusted the mirror to 200 different values of Θ within a range of about 3° and stored the reflected light images on the computer. From such image sequences, we obtained $R(\Theta)$ curves for each pixel of the CCD camera chip (resolution 768 by 576 pixels) and calculated the angle of resonance for each pixel by a fitting algorithm via Eq. 1. This revealed the three-dimensional surface topography of the deformed waveguide (Fig. 2C). From such measurements, we determined that the vertical accuracy of the method is in the nanometer range, whereas the lateral resolution, owing to the propagating nature of waveguides in the horizontal direction, is in the range of 1 to 2 μm.

We used this method to visualize and measure the force that a single cell can exert on an artificial surface (*16*). The two falcate conidia of *C. graminicola* (Fig. 3A) had been allowed to germinate and form dark, melanin-pigmented appressoria on the surface of the waveguide. The structures formed are indistinguishable from infection structures differentiated on the surface of a plant (Fig. 3B). In the corresponding reflected light image (Fig. 3C), two bright foci clearly correlate spatially with the locations of the two appressoria in Fig. 3A. Obviously, the thickness of the waveguide is changed at these sites, indicating exertion of vertical external force. From angle-resolved measurements, the cross section of a typical imprinted region under an appressorium—representing the shape of the penetration hypha forced into the waveguide—can be obtained (Fig. 3D). The typical vertical deformation observed in our experiments is ~10 nm, whereas the diameter of the penetration hypha at the appressorial base is ~2 μm. The area of the waveguide surrounding the penetration hypha is raised (Fig. 3D, inset), attesting to the tight adhesion of the appressorial base to the surface of the waveguide. As the waveguide is flexible, detachment of the appressorium due to insufficient adhesion would result in immediate extinction of the optical signal. This never occurred, indicating that the appressoria adhere tightly to the waveguides and that maximal forces were measured.

To quantify the forces that cause imprinting of the waveguide (Fig. 3D), we measured the elasticity of the waveguide by calibrating its optical response with defined external pressures. A thin tapered glass capillary with a diameter of 5 μm and known spring constant was mounted onto a micromanipulator that could be vertically adjusted with a precision of several micrometers. With this device, we exerted defined forces up to 35 μN on the same waveguides that were used to analyze the appressoria. We measured the depth of the indentation by the procedure described above and obtained a linear response of the waveguide over the whole range, corresponding to deformations up to 20 nm (Fig. 4A). The

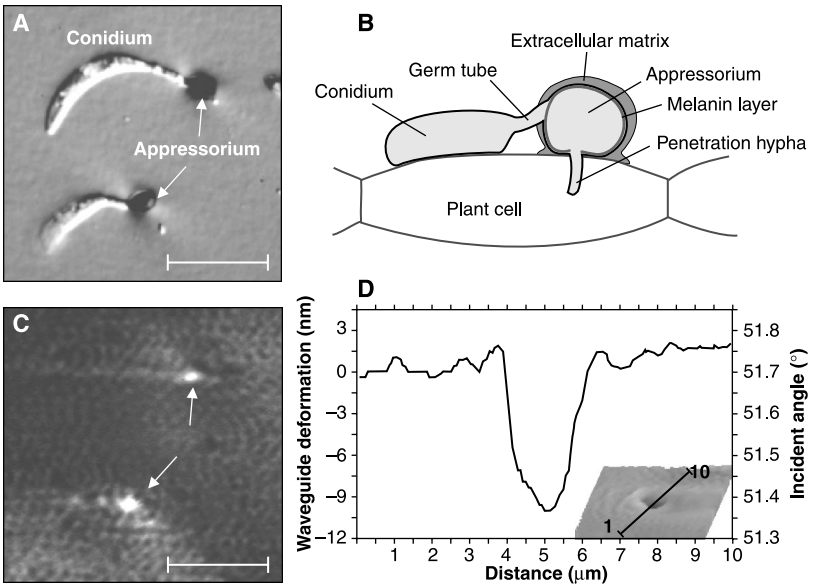

Fig. 3. (**A**) Light microscopic image of two conidia from *C. graminicola* forming appressoria on the aluminum surface of a waveguide. Scale bar, 10 μm. (**B**) Schematic drawing of a cross section through a conidium, a germ tube, and an appressorium infecting a plant cell (not to scale). The appressorium forms an extracellular matrix, which, together with adhesive beneath the appressorium, enables it to adhere to the plant surface. A melanin layer in the appressorial wall and synthesis of intracellular osmotically active material cause a buildup of turgor pressure necessary to penetrate the plant cell with the penetration hypha. (**C**) Reflected light image of the same area of the waveguide shown in (A). Two bright foci (arrows) clearly correlate spatially with the location of the two appressoria, indicating vertical external pressure. (**D**) Angle-resolved measurements reveal the waveguide topography (inset, lower right). A plot of the cross section of a typical imprinting region under an appressorium represents the shape of the penetration hypha forced into the waveguide. The typical vertical deformation is ~10 nm. The diameter of the penetration hypha at the appressorial base is ~2 μm.

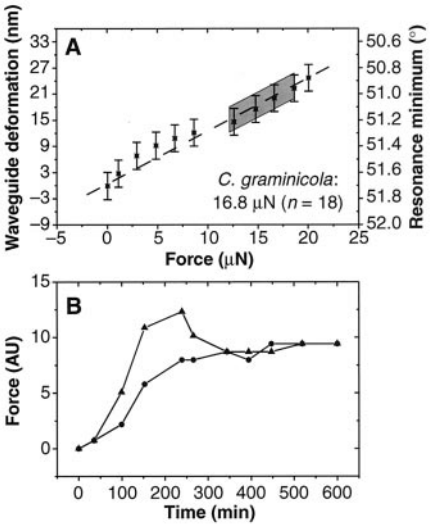

Fig. 4. (**A**) Calibration of the elastic response of the waveguide, using a glass capillary of known spring constant to exert defined forces. A linear response is obtained with forces up to about 20 μN. The right axis shows the angle of resonance, which corresponds to a local change in the thickness of the waveguide. Forces exerted by appressoria (shaded area) are in the range of 17 μN and are therefore in the linear range. (**B**) Temporal development of force exertion by two different appressoria (circles and triangles) during formation of the penetration hypha. Force exertion typically starts 100 min after appressoria formation and reaches a steady level after 300 min.

slope of the straight line shows the spring constant of the waveguide to be 1.63×10^3 N/m. From this value we calculated the force exerted by *C. graminicola* during the formation of the penetration hypha underneath the appressorium. Force exertion typically began 100 to 120 min after the formation of mature—that is, melanized—appressoria (determined by visual inspection with the light microscope) and reached a steady level after ~300 min (Fig. 4B). This level did not change for several hours. In 18 appressoria from four fresh preparations of conidia cultured onto four different waveguides, we measured a force of 16.8 μN (SD ±3.2 μN, range 8 to 25 μN).

Earlier studies used various techniques to measure the turgor pressure within an appressorium (*17, 18*). Given that the force is applied to an average diameter of 2 μm of the surface (Fig. 3D), which is in good agreement with the size of the penetration hyphae of *C. graminicola* as shown by transmission electron micrographs (*19*), the pressure within the appressorium would be 5.35 MPa. By comparison, Money (*20*) calculated that the pressure of 8.0 MPa found in appressoria of *M. grisea* corresponds to a force of 8 μN, assuming that the surface of the penetration peg in this fungus is ~1 μm^2. These forces should be sufficient to breach the cuticle and epidermal cell wall of mono- and dicotylous plants (*18*).

In addition to allowing precise determination of vertical forces exerted by single appressoria on an underlying surface, the waveguides have a relaxation time of less than 1 s and so may be used to monitor dynamic processes. Data obtained in this way may help to analyze the effect of antipenetrants, for example, chemical agents that interfere with melanin biosynthesis or the biogenesis of fungal cell walls. The elasticity of the waveguide can easily be varied by using different types of elastomers (*21*), allowing measurements of forces down to the nanonewton range.

References and Notes

1. E. C. Oerke, H. W. Dehne, F. Schönbeck, A. Weber, *Crop Production and Crop Protection* (Elsevier, Amsterdam, 1994).
2. J. C. De Jong, B. J. McCormack, N. Smirnoff, N. J. Talbot, *Nature* **389**, 244 (1997).
3. R. J. Howard and B. Valent, *Annu. Rev. Microbiol.* **50**, 491 (1996).
4. K. Mendgen, M. Hahn, H. Deising, *Annu. Rev. Phytopathol.* **34**, 367 (1996).
5. Y. Kubo *et al.*, *Appl. Environ. Microbiol.* **62**, 4340 (1996).
6. J. D. Walton, *Plant Physiol.* **104**, 1113 (1994).
7. A. Otto, *Phys. Stat. Sol.* **26**, K99 (1968).
8. E. Kretschmann and H. Raether, *Z. Naturforsch.* **23A**, 2135 (1968).
9. S. Herminghaus and P. Leiderer, *Appl. Phys. Lett.* **54**, 99 (1989).
10. C. R. Lavers, *Thin Solid Films* **289**, 133 (1996).
11. J. R. Sambles, G. W. Bradbery, F. Yang, *Contemp. Phys.* **32**, 173 (1991).
12. W. Hickel and W. Knoll, *Acta Metall.* **37**, 2141 (1989).
13. S. Herminghaus, C. Bechinger, W. Petersen, P. Leiderer, *Opt. Commun.* **112**, 16 (1994).
14. PDMS M30.000 was obtained from Sigma.
15. C. Bechinger, K.-F. Giebel, M. Schnell, P. Leiderer, H. B. Deising, M. Bastmeyer, data not shown.
16. *Colletotrichum graminicola* (Cesati) Wilson [teleomorph *Glomerella graminicola* (Politis)] was cultivated on 5% oatmeal medium, solidified with 1.2% agar. Cultures were incubated at room temperature under black-light lamps (Philips TL-D 36W/08). Conidia of three to five acervuli were suspended in distilled water and washed by repeated centrifugation to remove the germination self-inhibitor [B. Leite and R. L. Nicholson, *Exp. Mycol.* **16**, 76 (1992)]. The wild-type isolate of this fungus (CgM2) was obtained from R. L. Nicholson.
17. N. P. Money and R. J. Howard, *Fung. Genet. Biol.* **20**, 217 (1996).
18. R. J. Howard, M. A. Ferrari, D. H. Roach, N. P. Money, *Proc. Natl. Acad. Sci. U.S.A.* **88**, 11281 (1991).
19. D. J. Politis and H. Wheeler, *Physiol. Plant Pathol.* **3**, 465 (1973).
20. N. P. Money, *Can. J. Bot.* **73**, S96 (1995).
21. S. Herminghaus, M. Riedel, P. Leiderer, M. Bastmeyer, C. Stürmer, *Appl. Phys. Lett.* **70**, 22 (1997).

22. We thank M. A. Cahill for helpful comments on the text. Supported by grants from Deutsche Forschungsgemeinschaft (FOR 216/3), Optikzentrum Konstanz, and Fonds der Chemischen Industrie (M.B.).

24 May 1999; accepted 29 July 1999

Formation of Cycloidal Features on Europa

Gregory V. Hoppa,† B. Randall Tufts, Richard Greenberg, Paul E. Geissler

Cycloidal patterns are widely distributed on the surface of Jupiter's moon Europa. Tensile cracks may have developed such a pattern in response to diurnal variations in tidal stress in Europa's outer ice shell. When the tensile strength of the ice is reached, a crack may occur. Propagating cracks would move across an ever-changing stress field, following a curving path to a place and time where the tensile stress was insufficient to continue the propagation. A few hours later, when the stress at the end of the crack again exceeded the strength, propagation would continue in a new direction. Thus, one arcuate segment of the cycloidal chain would be produced during each day on Europa. For this model to work, the tensile strength of Europa's ice crust must be less than 40 kilopascals, and there must be a thick fluid layer below the ice to allow sufficient tidal amplitude.

Stress due to tidal deformation may drive global tectonics and the formation of linear features on Europa (*1–6*). However, the formation of the long chains of arcuate lineaments (or cycloids) on Europa has eluded explanation. These features have several arcuate segments, each ~100 km in length. The Voyager spacecraft observed an abundance of cycloidal ridges (called "flexi" in the nomenclature of the International Astronomical Union) at high southern latitudes (*1*, *7*, *8*), at which location the spacecraft's observing geometry and the photometric conditions favored visibility (Fig. 1).

The Galileo spacecraft has observed cycloidal features of different morphologic types. The

Lunar and Planetary Laboratory, 1629 East University Boulevard, University of Arizona, Tucson, AZ 85721–0092, USA.

†To whom correspondence should be addressed. E-mail: hoppa@lpl.arizona.edu

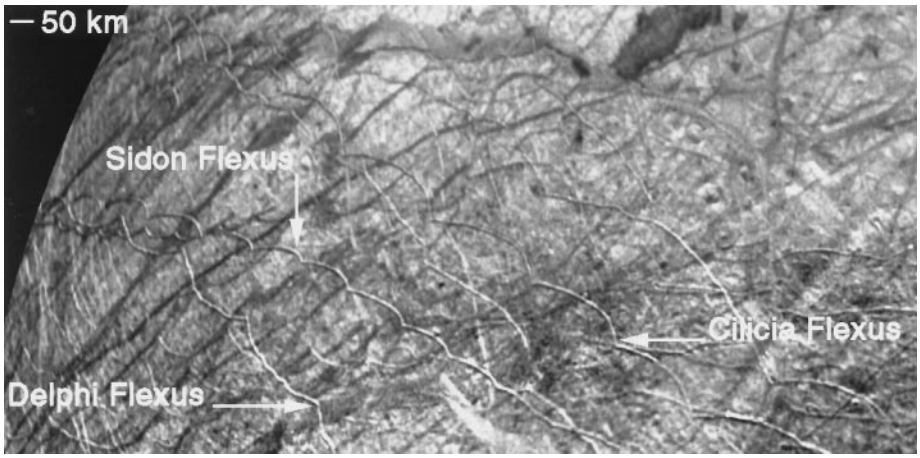

Fig. 1. Cycloidal ridges near Europa's south pole as viewed by the Voyager spacecraft (58°S, 166°W).